RP Current Trends In Applied Sciences (e-ISSN: 2583-7486)
Vol. 5, No. 2 (April – June 2026) pp. 95–103

RESEARCH PLATEAU PUBLISHERS

Cite this article: M.K. Das, R. Choudhury, V.K. Singh, S. Sardar, R.K. Lal, Hybrid metaheuristic optimization and comparative analysis of InGaAs/InP quantum well infrared photodetector for enhanced performance, *RP Cur. Tr. Appl. Sci.* **5** (2026) 95–103.

Original Research Article

Hybrid metaheuristic optimization and comparative analysis of InGaAs/InP quantum well infrared photodetector for enhanced performance

Mahendra Kumar Das, Rajveer Choudhury, Vishal Kumar Singh, Srijit Sardar, Rajesh Kumar Lal*

Department of Electronics and Communication Engineering, Birla Institute of Technology, Mesra, Off-campus Deoghar, 814142, India
*Corresponding author, E-mail: rklal@bitmesra.ac.in

ARTICLE HISTORY
Received: 15 April 2026
Revised: 27 May 2026
Accepted: 27 May 2026
Published: 13 June 2026

KEYWORDS
Quantum Well Photodetector; Heterostructure; Terahertz detection; Multi-objective optimization; Hybrid NSGA-II-PSO algorithm.

ABSTRACT
This work presents a hybrid metaheuristic optimization and comparative analysis of an InGaAs/InP-based quantum well photodetector (QWP) designed for terahertz (THz) long-wavelength infrared applications in the 8-12 μm spectral range. A comprehensive theoretical model is developed to enhance key performance parameters, including quantum efficiency, responsivity, detectivity, dark current, and noise equivalent power (NEP). The detector performance is strongly governed by structural parameters such as quantum well width and Indium mole fraction. Optimized results demonstrate peak absorption at 28.2 THz (10.6 μm) for a well width of 60 Å and Indium mole fraction of 0.34. At this optimized configuration, the device exhibits a high responsivity of 2.7 A/W, enhanced detectivity of 5.38×10^{11} cm$\sqrt{Hz}W^{-1}$, and a low dark current of 68 nA, indicating improved sensitivity and reduced noise performance. The corresponding NEP is significantly minimized due to the high detectivity of the device. To further improve performance, a multi-objective optimization framework is implemented using several metaheuristic algorithms, including Grey Wolf Optimization, Symbiotic Organism Search, Differential Evolution, Whale Optimization, Genetic Algorithm, Particle Swarm Optimization (PSO), and Ant Colony Optimization. The optimization simultaneously maximizes quantum efficiency, responsivity, and detectivity, while minimizing dark current and NEP. A comparative analysis reveals that a hybrid NSGA-II-PSO approach provides superior convergence and optimal trade-off characteristics, demonstrating its effectiveness for advanced QWP design and next-generation THz photodetection systems. The novelty of this work lies in the hybrid optimization-driven performance enhancement of InGaAs/InP QWPs, making them highly suitable for high-sensitivity THz communication and long-wavelength infrared detection applications.

1. Introduction

Quantum Well Infrared Photodetectors (QWIPs) have been extensively studied since the pioneering work of B. F. Levine, 1993, who established the fundamental principles of intersubband transitions and device operation for infrared detection [1]. Subsequent foundational contributions by H. C. Liu et al., 2006; Durante et al., 2007, further clarified the dependence of responsivity, absorption spectrum, and photoconductive gain on quantum well design parameters, providing a strong theoretical basis for device optimization [2, 3]. These classical studies demonstrated that QWIPs offer advantages such as spectral tunability, mature fabrication technology, and compatibility with semiconductor processing [4]. However, early designs were limited by relatively high dark current, narrow bandwidth and slower response times [1, 5].

In recent years, significant progress has been made toward improving QWIP performance through advanced material systems and structural engineering. For instance, Min-Su Park et al. demonstrated InGaAs/InP-based QWIPs integrated on silicon substrates, highlighting their potential for long-wavelength infrared detection with improved lattice matching and device uniformity [4]. Similarly, recent studies have explored broadband detection, enhanced detectivity, and reduced noise characteristics using novel heterostructures and quantum well configurations [4, 6]. Advances in modeling and simulation approaches, including TCAD-based analysis and analytical techniques, have further enabled accurate prediction and optimization of device performance [7]. Despite these developments, achieving a simultaneous improvement in responsivity, detectivity, bandwidth, and response time remains a challenging task, thereby motivating the need for systematic design and optimization of quantum well photodetectors for high-performance infrared applications.

Metaheuristic optimization techniques have recently been widely used for the design and performance enhancement of semiconductor photodetectors due to their effectiveness in handling complex, multi-parameter problems. Algorithms such as GA, PSO, DE, and GWO enable optimization of structural and material parameters to improve responsivity, detectivity, and reduce dark current. Among these, PSO offers fast convergence and ease of implementation, while GWO and DE provide higher accuracy in global optimization. Additionally, hybrid approaches combining these algorithms have been

explored to achieve better optimization efficiency and robust device performance [8–10].

In this work, an InGaAs/InP-based quantum well photodetector (QWP) is proposed for long-wavelength terahertz (THz) infrared detection in the 8–12 μm spectral range. The structure consists of an InGaAs quantum well sandwiched between InP barrier layers, forming a type-I heterostructure that provides strong carrier confinement and efficient intersubband transitions. The device performance is governed by key structural parameters such as quantum well width and Indium mole fraction, enabling precise spectral tuning. Energy states and transition characteristics are analyzed using the Transfer Matrix Method (TMM) and validated through TCAD-based simulations, ensuring both analytical and numerical accuracy. Furthermore, a hybrid metaheuristic optimization framework is employed to enhance responsivity, detectivity, and quantum efficiency while minimizing dark current and noise. The optimized structure exhibits peak operation at 28.2 THz (10.6 μm), demonstrating its suitability for high-sensitivity THz communication and long-wavelength infrared detection applications.

The novelty of this work lies in the integration of a physics-based InGaAs/InP quantum well photodetector model with a hybrid metaheuristic optimization framework for simultaneous multi-objective performance enhancement. Unlike conventional approaches that rely on parametric tuning, the proposed hybrid NSGA-II–PSO algorithm systematically identifies the optimal design parameters (L_w = 60 Å, L_b = 400 Å, x = 0.34), achieving an improved trade-off among responsivity, detectivity, dark current, and noise equivalent power. This combined modeling and optimization strategy enables enhanced sensitivity, faster response, and efficient long-wavelength THz detection, making the proposed device highly suitable for next-generation infrared communication systems.

The remainder of this paper is organized as follows: Section 2 presents the device structure and Theoretical formulation of the proposed InGaAs/InP QWP, Section 3 demonstrates results and discussions of hybrid NSGA-II–PSO optimization framework, Section 4 concludes the paper with key findings and future perspectives.

2. Theoretical formulation

The proposed InGaAs/InP-based QWP consists of an $In_xGa_{1-x}As$ quantum well sandwiched between two InP barrier layers, forming a type-I heterostructure as illustrated in Figure 1. The conduction band discontinuity at the InGaAs/InP interface creates a potential well that confines electrons within the well region (region II), while the adjacent barrier regions (regions I and III) restrict carrier leakage. Under incident radiation, electrons undergo intersubband transitions from the ground state (E_1) to the excited state (E_2), generating photocurrent through tunneling or thermionic emission mechanisms. The asymmetry introduced by the applied bias further facilitates carrier transport toward the contact layer, enabling efficient photodetection in the long-wavelength terahertz regime.

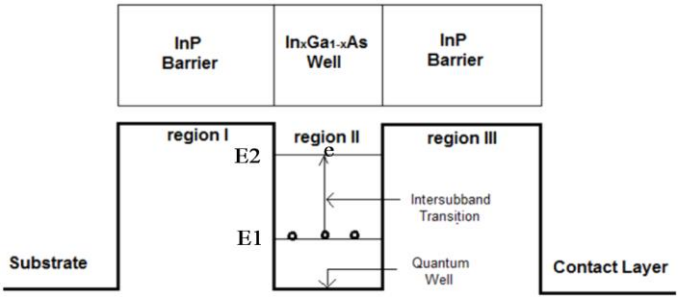

Figure 1: Energy band diagram of InGaAs/InP -based QWP [11].

2.1 Analytical modeling using the Transfer Matrix Method (TMM)

The quantized energy states of the proposed InGaAs/InP-based heterostructure, were solved by using one dimentional *Schrödinger equation* across the three regions, InP barrier (region I), InGaAs well (region II), and InP barrier (region III) as illustrated in figure 1 [12].

$$\frac{d}{dx}\left[\frac{1}{m^*(x,E)}\frac{d\psi(x)}{dx}\right] + \frac{2m^*(x,E)}{\hbar^2}[E - V(x)]\psi(x) = 0. \qquad (1)$$

Here $m^*(x,E)$ represents the position dependent effective mass and $V(x)$ represents the potential profile. The Transfer Matrix Method (TMM) was employed for solving the Schrödinger equation (1).

For a wave entering from region I and exiting region III, the transmission coefficient can be approximated as:

$$\tau = \frac{|Fe^{ik_1x}|^2}{|Ae^{ik_1x}|^2} = \frac{1}{|t_{11}|^2}. \qquad (2)$$

The solution of this equation gives the quantized energy eigenstates and the corresponding transition energy $\Delta E = E_2 - E_1$, further ΔE determines the absorption wavelength as

$$\lambda = \frac{hc}{\Delta E}. \qquad (3)$$

2.2 Numerical modeling and transport simulation Using TCAD

The optoelectronic performance of the proposed photodetector is analyzed using a TCAD-based finite element framework. The simulator solves the coupled Poisson, carrier continuity, and drift-diffusion transport equations to describe the interaction between electrostatic potential and carrier dynamics. These governing equations are iteratively solved using the Newton-Raphson method to obtain a self-consistent solution. In the present study, a quantum well width (L_w) = 60 Å barrier width of (L_b) =400 Å and Indium mole fraction of x = 0.34 were considered as the optimized structural parameters. The doping concentration is taken as 1.53×10^{24} cm^{-3}in the quantum well region and 1.33×10^{21} cm^{-3} in the barrier region, ensuring efficient carrier confinement and transport for enhanced device performance.

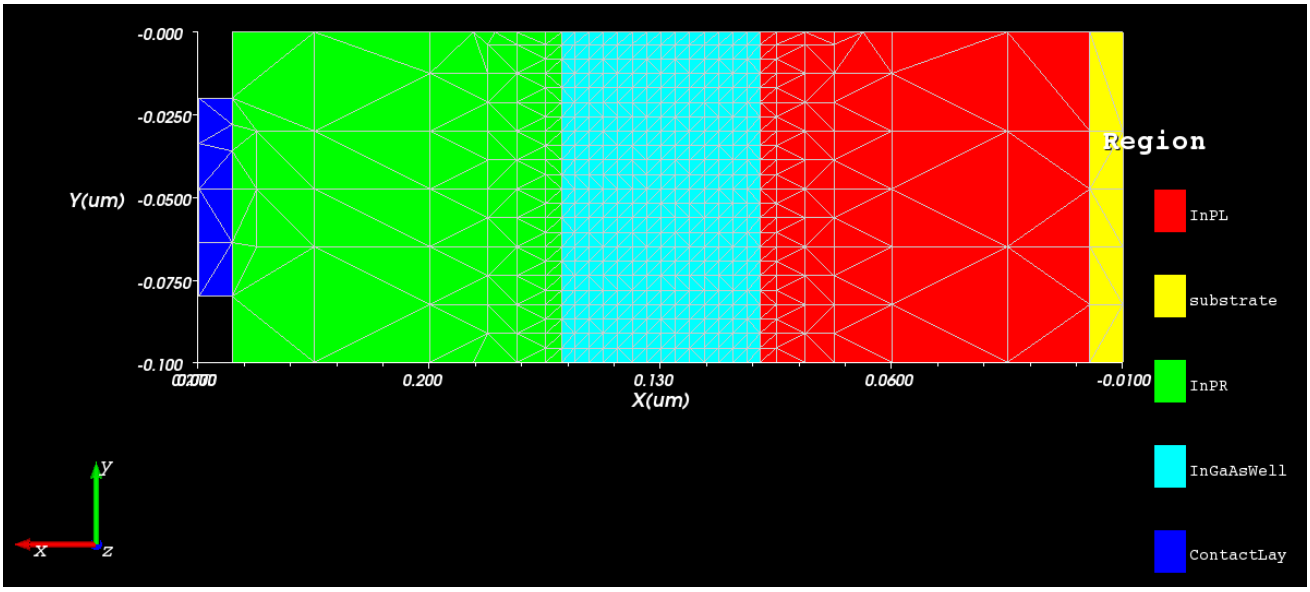

Figure 2: TCAD Simulated model of InGaAs/InP-based QWP.

Poisson's equation

The relation between charge density and electric field potential for the proposed QWP can be expressed from the Poisson's equation [7], as:

$$\rho \text{ total } (x) = N_{D1}(x) + N_{A2}(x) + \rho D(x) + \rho A(x) + \rho(x)\text{bound} \quad (4)$$

Here N_{D1} and N_{A2} represent the donor and acceptor densities of the InP barrier and InGaAs well regions, and $\rho(x)$ is the total charge density including donor (N_{D1}) and acceptor (N_{A2}) contributions respectively.

Continuity equation

The continuity equations for electron and hole can be expressed as

$$\mathcal{D}n\frac{d^2n(y)}{dy^2} - \wp(y) + G_{l,q} = 0 \text{ and}$$
$$\mathcal{D}p\frac{d^2p(y)}{dy^2} - \wp(y) + G_{l,q} = 0 \quad (5)$$

Here, $\wp(y)$ represents the combined influence of thermal generation and recombination processes. $G_{l,q}$ denotes the optical generation rate. $n(y)$ and $p(y)$ indicate the electron and hole concentrations, respectively, while $\mathcal{D}_n$ and $\mathcal{D}_p$ represents the electron and hole diffusion coefficients. The incident radiation is assumed to be uniform, and the TCAD simulator inherently solves both continuity equations [13, 14].

Transport equations

The current density for the proposed InGaAs/InP-based QWP can be expressed [15]

$$\mathcal{J} = q\mathcal{t}(\mathcal{A}1n + \mathcal{B}1n^2 + \mathcal{C}1n^3) + \mathcal{J}_{leakage} \quad (6)$$

where $\mathcal{A}1$, $\mathcal{B}1$, and $\mathcal{C}1$ correspond to SRH, radiative, and Auger recombination coefficients, respectively, $\mathcal{J}_{\text{leakage}}$ is the leakage current, and '$\mathcal{t}$' is active layer thickness of quantum well.

Device Photocurrent

The device photocurrent for the proposed study was expressed as the product of the carrier generation rate, charge, and the bias-dependent transport efficiency, $\xi(V)$ as [16]

$$I_D = q\frac{B_{n\lambda}}{hc}\sum_{i=1}^{N_R} w_R \int_0^{yi} Pi\alpha ie^{-\alpha_i y}\,\xi\,(V)dy \quad (7)$$

where B_n is the intensity of the nth beam, λ the source wavelength, WR the width of the ray, α_i represents the absorption coefficient, N_R the number of rays traced, *Pi* is the attenuation before the ray starts, *Yi* is the ray length.

Quantum Absorption Efficiency (η)

The overall quantum efficiency of the proposed photodetector was formulated in terms of conversion efficiency and photoconductive gain as [5].

$$\eta(\lambda, V) = \eta_{abs}\,\xi(V) \quad (8)$$

Detector Responsivity (*R*)

The detector responsivity were formulated as [5]

$$R\,(\lambda, V) = \eta_{abs}(\lambda)g(V)\frac{q\lambda}{hc} \quad (9)$$

$$g(V) = \frac{\tau_{life}}{\tau_{tr}(V)} = \frac{\tau_{life}Vd\,(V)}{Ld}$$

where $Vd\,(V) = \frac{\mu E}{\sqrt{1+\left(\frac{\mu E}{v_s}\right)^2}}$, here v_s is saturation velocity and *E* is the applied electric field

Dark Current (I_d)

The noise current generated by the photodetector without illumination is called dark current and for the proposed InGaAs/InP-based QWP, this is formulated as [17]

$$I_{dark} = Aen_{2D}V_d(v) \quad (10)$$

Detectivity (D)*

The detectivity of a detector with active area A_d, can be defined as the inverse of the Noise Equivalent Power (NEP) and the NEP of a detector strongly depends on the measurement of its bandwidth (Δf) [1, 18].

$$D^* = \frac{(Ad \times \Delta f)^{1/2}}{NEP} \quad \frac{cm\sqrt{Hz}}{W}, \tag{11}$$

where $NEP = \frac{I_n}{R}$, I_n= noise current and can be expressed as I_n=$\sqrt{4eGI_p\Delta f}$, G = optical gain and R = responsivity.

Optimization Algorithm

The performance optimization of the proposed InGaAs/InP-based QWP is formulated as a multi-objective problem to determine optimal structural and electrical parameters. The design variables were considered as

$$X = [L_w, L_b, x, V], \tag{12}$$

Subject to the constraints

$55\text{Å} \leq Lw \leq 62\text{Å}$, & $380\text{Å} \leq Lb \leq 420\text{Å}$, $0.29 \leq x \leq 0.36$, and $-3.5 \leq V \leq 3.5$

The objective is to simultaneously maximize quantum efficiency (η), responsivity (R), and detectivity (D*) while minimizing dark current (I_d) and noise equivalent power (NEP), expressed as [9, 19]

Maximize: η, R, & D^* and Minimize: I_d, NEP

Further, the normalized fitness function of the proposed device was defined as

$$F = \sum_{k=1}^{5} w_k . f_k' , \sum w_k = 1, \tag{13}$$

where f_k' are normalized objective functions.

Hybrid NSGA-II-PSO Algorithm

A hybrid NSGA-II-PSO algorithm is employed to solve the above problem. Initially, a population of candidate solutions is generated within the defined bounds. For each solution, the objective parameters are evaluated and fitness is computed [9, 19].

NSGA-II performs non-dominated sorting and crowding distance-based selection to identify elite solutions and maintain diversity. PSO is then used to update particle positions and velocities.

$$V_i^{t+1} = w.V_i^{t+1}c_1r_1\left(P_{best,i} - X_i^t\right) + c_2r_2\left(G_{best} - X_i^t\right) \tag{14}$$

$$\text{and } X_i^{t+1} = X_i^t + V_i^{t+1}. \tag{15}$$

In the above equations, . V_i^t and X_i^t represent the velocity and position of the i^{th} particle at iteration t respectively. V_i^{t+1} and X_i^{t+1}denote the updated velocity and position. The parameter w is the inertia weight that controls the influence of the previous velocity. c_1 and c_2 are the cognitive and social acceleration coefficients, respectively. r_1 and r_2 are uniformly distributed random numbers in the range [0,1]. $P_{best,i}$ is the best position previously visited by the i^{th} particle, while G_{best} represents the best solution obtained among all particles in the population.

The iterative process continues until convergence, yielding the optimal design parameters:

L_w = 60 Å, L_b = 400 Å, x = 0.34.

And yielding maximum responsivity and detectivity with minimum dark current and NEP, demonstrating superior performance compared to other optimization techniques.

Table 1: Material Properties used in the computational analysis [20-26].

Parameter	**Values**
Effective mass in the well	$m_w^* = 0.041m_0$
Effective mass in the barrier	$m_b^* = 0.0410 + 0.0835x)\text{m}_0$, where m_0 represents the electron rest mass
Potential Barrier Height	$\Delta E = \frac{V}{\_} = 0.75x$, *where* x represents the 'In' mole fraction
Carrier Density (well)	1.53×10^{24} cm^{-3}
Photoconductive gain	0.774
Lorentzian profile	$\Delta E = 5$ meV
Electron mobility(μ_e)(m^2/Vs)	10,000 cm^2·V^{-1}·s^{-1}
Electron affinity(eV)	4.23
Energy bandgap (E_g) (eV)	(1.344-0.738y+0.138y^2) eV
Absorption coefficient(α)	$\alpha_0 \exp(\frac{\delta(E-E0)}{ET})(\text{m}^{-1})$
Static Dielectric constant(ε_s)	12.5 +1.44Asy
High frequency dielectric constant	9.61 +2.0Asy
Lattice constant	5.869 Å

3. Results and discussion

Numerical simulations were carried out for a symmetrical and staggered $In_xGa_{1-x}As$/InP-based QWP structure using MATLAB. The computations were performed at a temperature of 77 K, with an applied electric field of 12.4 kV/cm across the device structure. The applied bias was varied between –3.5 V and +3.5 V, and the incident radiation was modeled to strike at an angle of 45° from the lower bandgap (InGaAs) side of the structure. The photodetector configuration under investigation is presented in Figure 1, and the various physical parameters used in the analysis were taken from the cited references [20-26] and are abstracted in Table 1.

The TMM was employed to calculate the quantized energy levels in the quantum well. These results were used to estimate the corresponding absorption wavelengths across the THz spectral region. The subband energy levels of the quantum well corresponding to the transmission coefficient peaks were plotted for well widths ranging from 55 Å to 62 Å and for Indium (In) mole fractions (x) varying between 0.29 and 0.36.

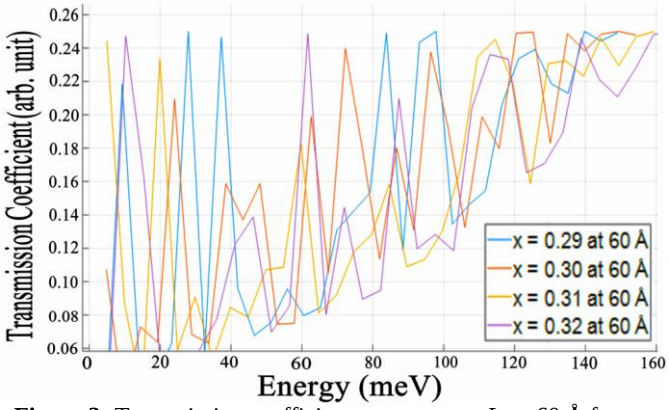

Figure 3: Transmission coefficient vs. energy at L_w = 60 Å for x = 0.29 to 0.32.

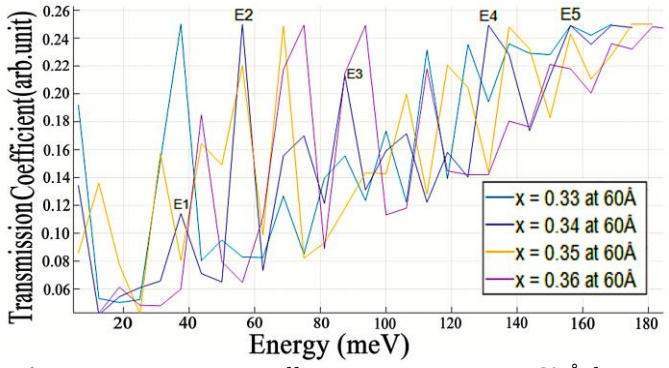

Figure 4: Transmission coefficient vs. energy at L_w = 60 Å for x = 0.33 to 0.36.

Figure 3, 4, and 5 present a detailed analysis of the transmission coefficient profiles, highlights the variation in Indium (In) composition in the well material $In_xGa_{1-x}As$ from x = 0.29 to 0.36 and its influence on the energy-dependent transmission at a quantum well width of 60 Å. The energy positions of the transmission peaks were then used to extract the corresponding sub-band energy levels, facilitating the estimation of the material's bandgap energy. This evaluated bandgap was then utilized to determine the operational wavelength of the proposed photodetector for different well widths and '*In*' mole fractions. The most prominent detection feature occurs for L_w=60 Å and x = 0.34, as illustrated in Figure 5 [27, 28].

Figure 6 presents the variation of wavelength corresponding to the calculated sub-band energy levels, derived from the transmission coefficient spectra, as a function of the Indium (*In*) mole fraction for quantum well widths of 55 Å, 56 Å, 58 Å, 60 Å, and 62 Å. The operating wavelengths for each mole fraction (x) and well width are summarized in Table 2. From Figure 6 and Table 2, it is evident that the $In_xGa_{1-x}As$/InP-based QWP exhibits operation around 28.2 THz, which corresponds to energy values of approximately 156.25 meV and 38.5 meV. At this configuration, the computed energy gap is 117.7 meV, and the associated wavelength for the conduction band offset is about 10.58 µm, as indicated in Figure 5. In this case, the detector structure has a well width of 60 Å and an Indium mole fraction of 0.34. The obtained results show good agreement with previously reported studies [4, 29, 30]. Furthermore, the proposed InGaAs/InP-based QWP structure demonstrates strong correlation with the experimental data reported by Min-Su Park et al. (2018), confirming its feasibility for practical fabrication and real-world applications [4].

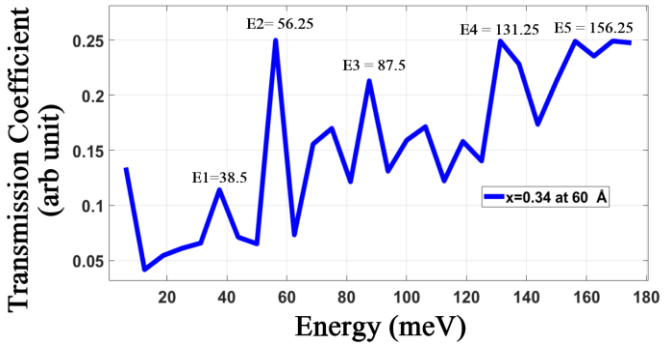

Figure 5: Transmission coefficient vs. energy at L_w = 60 Å for 'In' mole fraction, x = 0.34.

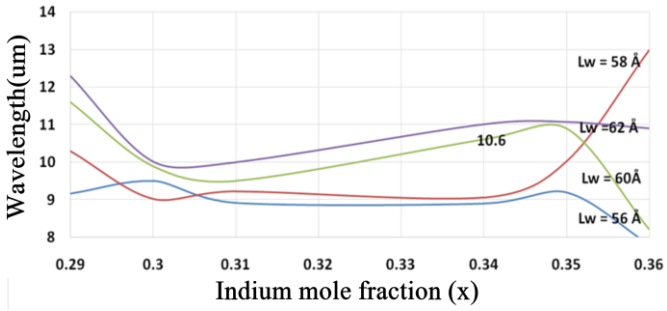

Figure 6: Wavelength (λ) vs. 'In' mole fraction (x) at well widths (L_w) 56 Å, 58 Å, 60 Å, and 62 Å.

Table 2: Absorption efficiency, responsivity, and wavelength values for various well widths (L_w) and Indium mole fractions (x), derived from Figures 3 to 8

Well width (L_w in Å)	Indium mole fraction (x)	Wavelength λ_{peak} (µm)	Absorption Efficiency (η) cm^{-1}	Responsivity (A/W)
55	0.31	8.9	700	2.52
56	0.31	9.02	760	2.54
58	0.29	9.2	850	2.50
60	0.34	10.6	945	2.70
62	0.35	11.6	997	2.78

Hence the variation in operating wavelength with Indium mole fraction and quantum well width demonstrates the strong dependence of the detector's spectral response on structural parameters. Increasing Indium concentration leads to a narrower bandgap and hence a shift toward longer wavelengths, while decreasing well width enhances quantum confinement, producing a blueshift. This tunability highlights the potential of $In_xGa_{1-x}As$/InP quantum well structures for application in the terahertz and mid-infrared spectral regions, where wavelength selectivity is critical for device optimization. The computed results align closely with earlier theoretical and experimental findings, validating the simulation approach [31, 32].

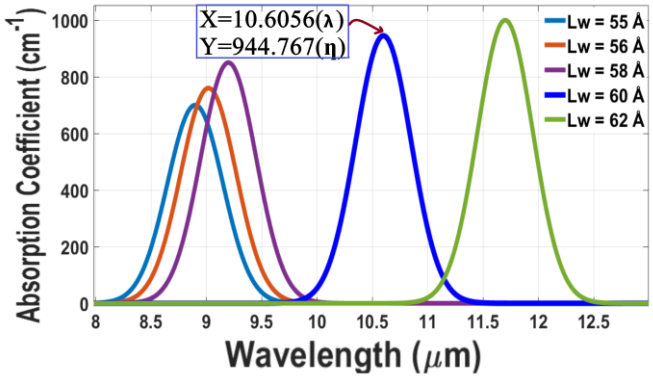

Figure 7: Absorption coefficient (η) vs. wavelength (λ) at various well width L_w = 55 Å to 62 Å and at 'In' mole fraction x = 0.34.

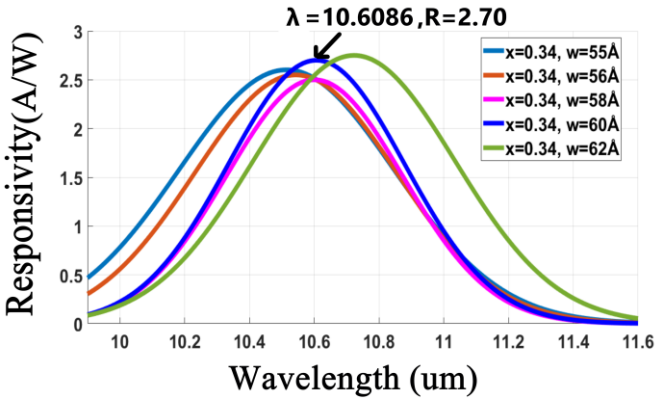

Figure 8: Responsivity vs. wavelength at various well width and 'In' mole fraction at bias voltage -3V.

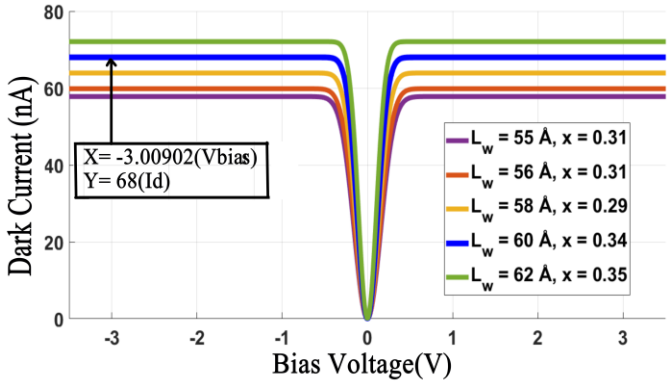

Figure 9: Dark Current vs. bias voltage at different 'In' mole fraction and well width (L_w).

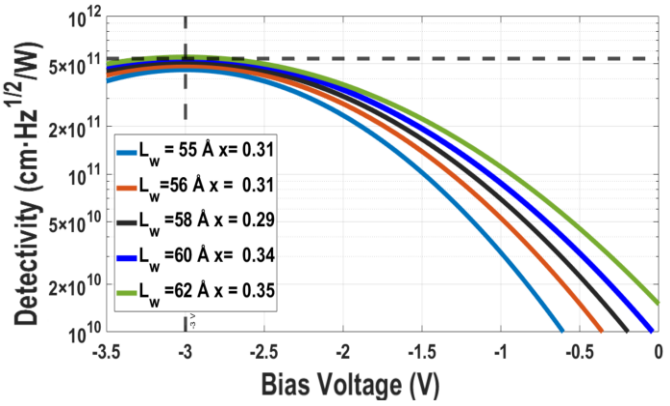

Figure 10: Detectivity vs. bias voltage at different 'In' mole fraction and well width (L_w).

In this study, Figure 7 presents the absorption efficiency of the proposed structure, simulated as a function of wavelength for different well widths ranging from 55 Å to 62 Å, while keeping the Indium (In) composition fixed at 0.34. The analysis reveals that the absorption efficiency peak tends to increase with increasing quantum well width [5, 33]. For L_w= 60 Å, the maximum absorption efficiency is obtained for an Indium mole fraction of x = 0.34, corresponding to a wavelength of 10.6 μm with an efficiency value of 945 cm-1 [34].

Figure 8 presents the variation of responsivity (R) with operating wavelength (λ), highlighting the influence of quantum well width and Indium mole fraction (x) on the overall detector performance. The analysis shows that a comparatively high responsivity of 2.7 A/W is obtained at x = 0.34 under a bias voltage of -3.0 V. Such enhanced responsivity can be achieved through the careful optimization of both the Indium composition and the quantum well width. Furthermore, the results indicate that the peak responsivity increases progressively with larger well widths and higher Indium concentrations [29].

Further, Figure 9 shows the variation of dark current with applied bias for different Indium concentrations and quantum well widths. For the proposed QWP structure, a low dark current of 68 nA is obtained at an applied bias of -3.0 V for x = 0.34 and L_w = 60 Å. This result is consistent with the expected characteristics of the $In_xGa_{1-x}As$/InP quantum well photodetector, considering both the material parameters and the applied bias conditions, and aligns closely with values reported in earlier literatures [6, 26].

Figure 10 illustrates the specific detectivity that can be achieved for $In_xGa_{1-x}As$/InP QWP for various selected well width and 'In' mole fraction. High detectivity indicates the potentiality of a photodetector to detect weak incident optical signals. Detectivity and responsivity of any photodetector are directly related to each other according to the mathematical expression (18 & 19). For the photosensitive area A_d and the bandwidth(Δf), this is usually considered as *1 Hz* for the calculation [35]. It can be concluded from equations (15, 16, & 19) that low dark current and high responsivity are desired for any photodetector to manifest high detectivity. Figure 10 shows the estimated detectivity of the proposed device as a function of reverse bias voltage between -3.5 to 0 volt variation. For a specific wavelength of 10.6 um the simulated result of detectivity is obtained as 5.38×10^{11} $cm\sqrt{Hz}W^{-1}$ under -3 volt bias and at L_w= 60 Å and x = 0.34, represented in Figure 11. A substantial enhancement in specific detectivity is observed in this work compared to previously reported quantum well photodetectors. [6, 29].

Furthermore, the calculated values of dark current, and detectivity, for different quantum well widths (L_w) and Indium molar concentrations (x) are listed in Table 3, derived from the results shown in the preceding figures. A comparison of Tables 2 and 3 indicates that, for the proposed QWP structure, an increase in well width leads to a corresponding rise in the absorption coefficient, and with a higher Indium content, the peak wavelength shifts toward shorter wavelength values within the terahertz region. For x = 0.34, the detector operates at 28.2 THz (10.6 μm), resulting in enhanced responsivity, and detectivity, along with reduced dark current.

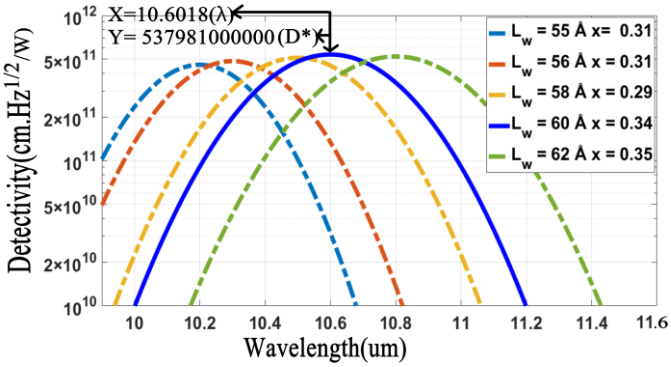

Figure 11: Detectivity vs. wavelength under the bias of -3.0 V at 77K.

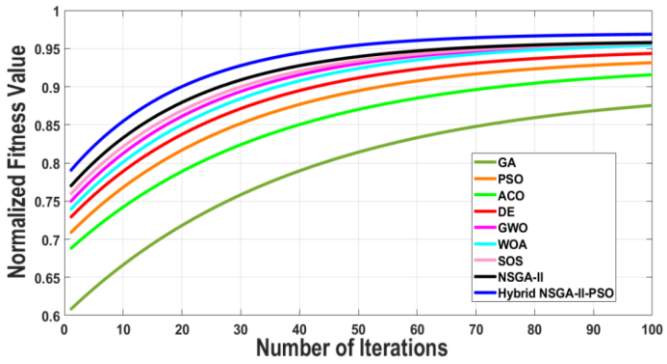

Figure 12: Convergence of metaheuristic algorithms showing superior performance of the Hybrid NSGA-II–PSO.

Table 3: Dark Current, and Detectivity values, for various well widths (L_w) and Indium mole fractions (x), derived from Figs. 9 to 11.

Well width (L_w in Å)	Indium mole fraction (x)	Wavelength λ_{peak} (μm)	Dark current (nA)	Detectivity (cm$\sqrt{Hz}W^{-1}$)
55	0.31	8.9	58	0.32×10^{11}
56	0.31	9.02	60	1.35×10^{11}
58	0.29	9.2	63	4.48×10^{11}
60	0.34	10.6	68	5.38×10^{11}
62	0.35	11.6	72	3.52×10^{11}

To further enhance the device performance, a comprehensive multi-objective optimization study was carried out using various metaheuristic algorithms, including GA, PSO, DE, GWO, WOA, SOS, and ACO. The optimization simultaneously maximizes quantum efficiency, responsivity, and detectivity, while minimizing dark current and noise equivalent power (NEP) [19, 36-40]. The comparative analysis reveals that all algorithms converge toward improved device performance; however, noticeable variations are observed in convergence accuracy and stability. Among them, the hybrid NSGA-II–PSO algorithm demonstrates superior optimization capability by effectively balancing exploration and exploitation, leading to the optimal design parameters L_w = 60 Å, L_b = 400 Å, and x = 0.34. At this configuration, the device achieves a high responsivity of 2.7 A/W, enhanced detectivity of 5.38×10^{11} cm$\sqrt{Hz}W^{-1}$, and a reduced dark current of 68 nA, along with minimized NEP. These results confirm the effectiveness of the hybrid optimization approach in achieving an optimal trade-off among conflicting performance parameters for high-sensitivity THz photodetection.

Table 4. Comparative evaluation of device performance parameters obtained using various metaheuristic optimization algorithms for the proposed InGaAs/InP QWP.

Algorithm	Absorption Efficiency (η) cm^{-1}	Responsivity (A/W)	Detectivity (cm$\sqrt{Hz}W^{-1}$)	Dark current (nA)	NEP (w/$\sqrt{Hz}$)	Convergence
GA	900	2.45	4.60×10^{11}	82	2.25×10^{-12}	slow
PSO	920	2.56	4.86×10^{11}	77	2.10×10^{-12}	good
ACO	928	2.51	4.72×10^{11}	80	2.18×10^{-12}	moderate
DE	936	2.61	4.88×10^{11}	74	2.02×10^{-12}	good
GWO	932	2.63	5.08×10^{11}	73	1.95×10^{-12}	good
WOA	937	2.58	5.02×10^{11}	74	1.98×10^{-12}	good
SOS	940	2.65	5.27×10^{11}	71	1.92×10^{-12}	better
NSGA-II	942	2.68	5.35×10^{11}	69	1.85×10^{-12}	Very good
Hybrid NSGA-II–PSO	946	2.70	5.39×10^{11}	68	1.82×10^{-12}	Best

From Table 4, the optimized device parameters (L_w = 60 Å and x = 0.34) obtained through the hybrid NSGA-II–PSO algorithm yield a maximum responsivity of 2.7 A/W, detectivity of 5.39 $\times10^{11}$ cm$\sqrt{Hz}$.W^{-1}, and a minimum dark current of 68 nA. Comparative analysis with other metaheuristic algorithms demonstrates that they converge to sub-optimal solutions with relatively lower responsivity and detectivity and higher noise characteristics. The employed optimization algorithms are based on well-established metaheuristic techniques reported in literature [19, 36-40].

Table 5: Comparison of optimized well width, barrier width, and Indium mole fraction for the proposed InGaAs/InP QWP using different metaheuristic algorithms.

Algorithm	Well width (L_w)	Barrier width (L_b)	Mole fraction (x)	Normalised fitness
GA	55-62	380	0.30-0.36	0.89
PSO	57-61	390	0.31-0.36	0.94
ACO	58-61	385	0.30-0.35	0.92
DE	59-61	385	0.32-0.34	0.95
GWO	57-62	397	0.32-0.36	0.96
WOA	57-61	395	0.32-0.35	0.93
SOS	59-63	402	0.33-0.34	0.96
NSGA-II	58-60	398	0.33-0.34	0.97
Hybrid NSGA-II–PSO	60±1	401	0.34	0.98

Table 5 presents the optimized structural parameters of the proposed QWP obtained using different metaheuristic algorithms. It is observed that the hybrid NSGA-II–PSO approach converges to the optimal design with L_w = 60±1 Å, L_b = 401 Å, and x = 0.34, achieving the highest normalized fitness value, while other algorithms exhibit wider parameter variations and comparatively lower fitness as shows by Figure 12.

Table 6: Comparison of the present study with the contemporary work.

Ref.	Material System	L_w (Å)	Molar Fraction (x)	Bias (V)	Opr. Freq. (THz)	Temp. (K)	Responsivity (A/W)	Detectivity ($\mathrm{cm}\sqrt{Hz}W^{-1}$)	Dark Current
Min-Su Park et al [4]	InGaAs/ InP	56	0.53	-0.7	28.2	77	-----	------	8.5×10^{-8} A
B.F. Levine et al [29]	GaAs/AlGaAs	38	0.22		29.3	77	0.35	1x10 ^{11}	10 uA
Jingyi Wang et al [6]	InGaAs/InP	-----	0.53	-1.0	149.8	293	-----	1.59×10^{10}	3.48×10^{-4} A/cm^2
Mihail Giannopoulos [41]	GaAs/AlGaAs	70	0.20	-4.0	30	10	0.38	3.5×10^{11}	1.0×10^{-9} A
S.V. Bandara et al [42]	GaAs/AlGaAs	150	0.06	-----	8.9	7	---	1.8×10^{11}	----
Proposed work	InGaAs/ InP	60	0.34	-3.5 to +3.5	28.2	77	2.7	5.38×10^{11}	68 nA

Table 6 presents a comparative analysis of the proposed InGaAs/InP QWP with previously reported photodetectors in terms of structural parameters and key performance metrics. It is observed that the proposed device achieves a significantly higher responsivity of 2.7 A/W and enhanced detectivity of 5.38×10^{11} $\mathrm{cm}\sqrt{Hz}W^{-1}$, along with a low dark current of 68 nA at 77 K. Compared to existing works, the proposed structure demonstrates superior performance and improved sensitivity, highlighting the effectiveness of the optimized design for high-performance terahertz infrared detection.

4. Conclusions

In this work, an InGaAs/InP-based quantum well photodetector (QWP) has been designed and analyzed for long-wavelength terahertz infrared detection in the 8–12 μm range. The device performance was evaluated using both analytical modeling via the Transfer Matrix Method (TMM) and numerical simulation through TCAD, ensuring accurate prediction of energy states and carrier transport. The results indicate that the detector characteristics are strongly influenced by structural parameters, with an optimal configuration of L_w = 60 Å and x = 0.34 yielding a high responsivity of 2.7 A/W, enhanced detectivity of 5.38×10^{11} $\mathrm{cm}\sqrt{Hz}W^{-1}$, and a low dark current of 68 nA. A comprehensive multi-objective optimization study confirms that the hybrid NSGA-II–PSO algorithm provides superior convergence and an optimal trade-off among performance parameters compared to other metaheuristic techniques. The novelty of this work lies in the integration of a physics-based QWP model with a hybrid metaheuristic optimization framework for simultaneous performance enhancement. However, the study is limited to simulation-based analysis under ideal conditions without experimental validation. Future work will focus on experimental realization and validation of the proposed device, along with the exploration of advanced material systems and inclusion of temperature-dependent effects and fabrication constraints to further improve practical applicability.

Authors' contributions

The author read and approved the final manuscript.

Conflicts of interest

The author declares no conflict of interest.

Funding

This research received no external funding.

Data availability

No new data were created.

References

[1] B.F. Levine, Quantum-well infrared photodetectors, *J. Appl. Phys*. **74** (1993) R1–R81.
[2] F. Durante, P. Alves, G. Karunasiri, N. Hanson, M. Byloos, H.C. Liu, A. Bezinger, M. Buchanan, NIR, MWIR and LWIR quantum well infrared photodetector using interband and intersubband transitions, *Infrared Phys. Technol*. **50** (2007).
[3] M. Park, M. Rezaei, I. Nia, R. Brown, S. Bianconi, C.L. Tan, H. Mohseni, InGaAs/InP quantum well infrared photodetector integrated on Si substrate by Mo/Au metal-assisted wafer bonding, *Opt. Mater. Express* **8** (2018) 413.
[4] H.C. Liu, Dependence of absorption spectrum and responsivity on the upper state position in quantum well intersubband photodetector, *J. Appl. Phys*. **73** (1993) 3062–3067.
[5] J. Wang, Z. Xie, L. Zhu, X. Zou, InP-based broadband photodetectors with InGaAs/GaAsSb type-II superlattice, *IEEE Electron Device Lett*. **43** (2022).
[6] V.K. Devarakonda, A.D. Dwivedi, A. Pandey, P. Chakrabarti, Performance analysis of N+-CdTe/n0-$Hg_{0.824675}Cd_{0.175325}Te$/p+-$Hg_{0.824675}Cd_{0.175325}Te$ n-i-p photodetector operating at 30 μm wavelength for terahertz applications, *Opt. Quantum Electron*. **52** (2020) 340.
[7] D.E. Goldberg, J.H. Holland, Genetic algorithms and machine learning, *Mach. Learn*. **3** (1988) 95–99.
[8] M. Dorigo, L.M. Gambardella, Ant colony system: A cooperative learning approach to the travelling salesman problem, *IEEE Trans. Evol. Comput*. **1** (1997) 53–66.

[9] M. Rashidi, A. Asgari, Modeling of novel lateral AlGaAs/GaAs quantum well solar cell, *Mesoscale Nanoscale Phys*. (2016) 11581288.

[10] P. Paramasivam, N. Gowthaman, V.M. Srivastava, Self-consistent analysis for optimization of AlGaAs/GaAs based heterostructure, *J. Electr. Eng. Technol*. **19** (2024) 4469–4483.

[11] M.K. Das, V.K. Yadav, R.K. Lal, Modeling and simulation of a GaAs/AlGaAs quantum well photodetector for terahertz application, *J. Comput. Electron*. **26** (2025).

[12] S.R. Andrews, B.A. Miller, Experimental and theoretical studies of the performance of quantum well infrared photodetectors, *J. Appl. Phys*. **70** (1991) 993–1003.

[13] B.F. Levine, K.K. Choi, C.G. Bethea, J. Walker, R.J. Malik, New 10 μm infrared detector using inter-sub-band absorption in resonant tunneling GaAlAs superlattices, *Appl. Phys. Lett*. **50** (1987) 1092–1094.

[14] K. Deb, A. Pratap, S. Agarwal, T. Meyarivan, A fast and elitist multi-objective genetic algorithm: NSGA-II, *IEEE Trans. Evol. Comput*. **6** (2002) 182–197.

[15] Y. Takeda, A. Sasaki, Y. Imamura, T. Takagi, Electron mobility and energy gap of $In_{0.53}Ga_{0.47}As$ on InP substrate, *J. Appl. Phys*. **47** (1976) 5405–5407.

[16] T.P. Pearsall, R. Bisaro, R. Ansel, P. Merenda, The growth of $Ga_xIn_{1-x}As$ on (100) InP by liquid-phase epitaxy, *Appl. Phys. Lett*. **32** (1978) 497–499.

[17] R. Nicholas, J.C. Portal, C. Houlbert, P. Perrier, T.P. Pearsall, An experimental determination of the effective masses for $Ga_xIn_{1-x}As_yP_{1-y}$ alloys grown on InP, *Appl. Phys. Lett*. **34** (1979) 492–494.

[18] C. Hermann, T.P. Pearsall, P. Thomas, Optical pumping and the valence-band light-hole effective mass in $Ga_xIn_{1-x}As_yP_{1-y}$ (y = 2.2x), *Appl. Phys. Lett*. **38** (1981) 450–452.

[19] T.P. Pearsall, J.P. Hirtz, The carrier mobilities in $Ga_{0.47}In_{0.53}As$ grown by organo-metallic CVD and liquid-phase epitaxy, *J. Cryst. Growth* **54** (1981) 127–131.

[20] N. Kotera, K. Tanaka, Determination of electron effective mass from optical transition energy in InGaAs/InAlAs quantum wells, *Physica E* **32** (2006) 199–202.

[21] Y. Arslan, T. Colakoglu, C. Besikci, Diffraction-grating-coupled high quantum efficiency InP/InGaAs quantum well infrared photodetector focal plane array, *IEEE J. Quantum Electron*. **49** (2013) 186–195.

[22] D.K. Sengupta, G.E. Stillman, Growth and characterization of n-type InP/InGaAs quantum well-infrared photodetectors for response at 8.93 μm, *J. Electron. Mater*. **26** (1997) 1376–1381.

[23] B.F. Levine, G. Hasnain, C.G. Bethea, N. Chand, Broadband 8–12 μm high sensitivity GaAs quantum well infrared photodetector, *Appl. Phys. Lett*. **54** (1989) 2704.

[24] K.K. Chow, Detection wavelength of quantum well-infrared photodetectors, *J. Appl. Phys*. **73** (1993) 5230–5236.

[25] C. Besikci, High-x InP/$In_xGa_{1-x}As$ quantum well infrared photodetector, *Infrared Phys. Technol*. **95** (2018) 52–57.

[26] S. Tyagi, P. Saxena, R. Kumar, Numerical simulation of $In_xGa_{1-x}As$/InP PIN photodetector for optimum performance at 298 K, *Opt. Quantum Electron*. **52** (2020).

[27] B.F. Levine, A. Zussman, Photo-excited escape probability, optical gain, and noise in QWIP, *J. Appl. Phys*. **72** (1992) 4429–4443.

[28] M. Razeghi, M. Erdtmann, C. Jelen, J. Diaz, F. Guastavino, Y.S. Park, High performance long wavelength infrared quantum well infrared photodetectors, *Def. Sci. J*. **51** (2001) 35–52.

[29] Y. Lin, K.H. Lee, B. Son, C.S. Tan, Low-power and high detectivity Ge photodiodes by in-situ heavy As doping during Ge-on-Si seed layer growth, *Opt. Express* **29** (2021) 2940–2952.

[30] R. Storn, K. Price, Differential evolution – A simple and efficient heuristic for global optimization over continuous spaces, *J. Glob. Optim.* **11** (1997) 341–359.

[31] S. Mirjalili, S.M. Mirjalili, A. Lewis, Grey wolf optimizer, *Adv. Eng. Softw*. **69** (2014) 46–61.

[32] S. Mirjalili, A. Lewis, The whale optimization algorithm, *Adv. Eng. Softw*. **95** (2016) 51–67.

[33] M.Y. Cheng, D. Prayogo, Symbiotic organisms search: A new metaheuristic optimization algorithm, *Comput. Struct*. **139** (2014) 98–112.

[34] H. Schneider, H.C. Liu, Quantum Well Infrared Photodetectors: Physics and Applications, Springer, Berlin (2006).

[35] M. Fox, R. Ispasoiu, Quantum Wells, Superlattices, and Band-Gap Engineering, in: Handbook of Electronic and Photonic Materials, Springer, Berlin (2017).

[36] E. O'Reilly, Quantum Theory of Solids, Taylor and Francis, London (2002).

[37] D.A. Neamen, Semiconductor Physics and Devices: Basic Principles, 4th edn., McGraw-Hill, New York (2012).

[38] H.C. Liu, F. Capasso, E.R. Weber, R.K. Willardson, Intersubband Transitions in Quantum Wells: Physics and Device Applications, Semiconductors and Semimetals, Vol. 62, 1st edn., Academic Press (1999).

[39] E.G. Talbi, Metaheuristics: From Design to Implementation, John Wiley & Sons, New Jersey (2009).

[40] J. Kennedy, R. Eberhart, Particle swarm optimization, Proc. ICNN'95 International Conference on Neural Networks, Perth, Australia, Vol. 4 (1995) pp. 1942–1948.

[41] M. Giannopoulos, Tunable bandwidth quantum well infrared photo detector, Master's Thesis, Naval Postgraduate School, Monterey, California (2003).

[42] S.V. Bandara, S.D. Gunapala, S. Rafol, J.K. Liu, GaAs/AlGaAs multi-quantum-well based far infrared detectors for astronomy application, Jet Propulsion Laboratory, California (2021).